COBEM 2021 26th International Congress of Mechanical Engineering
November 22-26, 2021, Virtual Congress, Brazil

COB-2021-1166
NUMERICAL AND EXPERIMENTAL INVESTIGATION OF THE HYDRODYNAMICS OF A SEMISUBMERSIBLE PLATFORM MODEL FOR FLOATING OFFSHORE WIND TURBINES

André Xavier Scopel
Daniel Francisconi Oliveira
Lucas Henrique Souza do Carmo
Pedro Cardoso de Mello
Escola Politécnica da Universidade de São Paulo, Av. Prof. Luciano Gualberto, 380 - Butantã, São Paulo - SP, 05508-010, Brasil
andrexscopel@usp.br, daniel.francisconi.oliveira@usp.br, lucas.carmo@usp.br, pcmello@usp.br

Edgard Malta
Technomar Av. Pedroso de Moaris, 631 - Pinheiros, São Paulo – SP, 05419-905, Brasil
edgard@technomar.com.br

Guilherme Rosa Franzini
Alexandre Nicolaos Simos
Escola Politécnica da Universidade de São Paulo, Av. Prof. Luciano Gualberto, 380 - Butantã, São Paulo - SP, 05508-010, Brasil
gfranzini@usp.br, alesimos@usp.br

Rodolfo Trentin Gonçalves
Hideyuki Suzuki
The University of Tokyo, 7 Chome-3-1 Hongo, Bunkyo City, Tokyo 113-8654, Japão
goncalves@orca.k.u-tokyo.ac.jp, suzukih@sys.t.u-tokyo.ac.jp

Bruno Souza Carmo
Escola Politécnica da Universidade de São Paulo, Av. Prof. Luciano Gualberto, 380 - Butantã, São Paulo - SP, 05508-010, Brasil
bruno.carmo@usp.br

Abstract. *This study focuses on the hydrodynamics of a semisubmersible platform model, designed to support a floating offshore wind turbine. The model was subject to forced sinusoidal motion tests in a water tank experimental facility, for a range of amplitudes and periods. Forces and displacements were measured so we could calculate hydrodynamic drag and inertia coefficients. Next, we performed numerical simulations using computational fluid dynamics (CFD) of the same setup. After the validation of the computational model and postprocessing procedures through the comparison of the force results, we analyzed the vorticity and pressure fields in order to relate the behavior of the hydrodynamic forces to characteristics of the flow field. We finally draw conclusions with respect to the strengths and limitations of these approaches and their potential as analysis and design tools of other floating offshore wind turbine platforms.*

Keywords: *Hydrodynamics, semisubmersible platform, floating offshore wind turbines, numerical simulations, water tank*

1. INTRODUCTION

As the global energy consumption is continuously growing, the search for clean and renewable sources has increasingly become one of the main concerns of modern engineering, and they now represent around one quarter of the total final electricity consumption worldwide. In particular, wind energy presents itself as one of the most attractive alternatives and represents now a rising significant parcel of the total energy generated around the world, showing, in 2020, a year-over-year growth of 53% (Lee, et al., 2021). While most of the new installed turbines are still onshore, the past few years has witnessed a continuous growth of the offshore parcel, which tends to increase with the development of new technologies. (Lee, et al., 2021).

Offshore projects were once too expensive and not viable, but, with new technologies, it is possible to build larger turbines that go even deeper into the ocean. This reduces the cost of installation and maintenance per GW of energy produced while eliminating the onshore installation problems like visual and noise impact, and available space. (Sun, Huang, & Wu, 2012), (Bilgili, Yasar, & Simsek, 2011).

Therefore, it becomes crucial to understand and predict the behavior of the wind turbines in the ocean environment, accounting for current and waves over the platform. Carmo, et al. (2020) and Amaral, et al. (2021) performed experiments to simulate these conditions, acquiring the inline force responses for the platform under forced oscillating motion. The goal of this study is to evaluate a numerical method to describe the same conditions tested in the experiments, which could provide further insights into the flow patterns and force coefficients agreement.

The considered geometry was the Jappaku floating wind turbine, which consists of a semi-submersible hull with a 15 m diameter central column attached to three 9 m diameter columns arranged as an equilateral triangle (Figure 1). Table 1 shows all the dimensions.

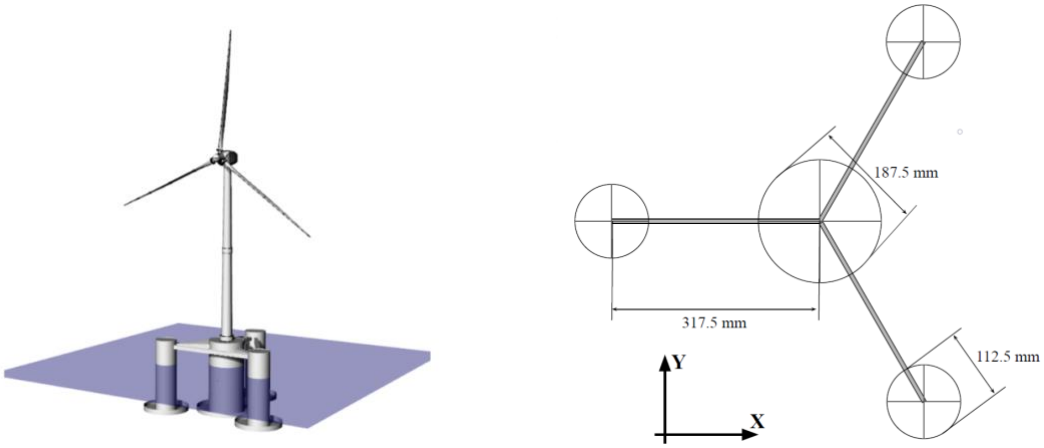

Figure 1. Geometry of the studied wind turbine.

Table 1. Main platform properties

	Full scale	Model Scale (1:80)
Diameter of main column	15.0 m	187.5 mm
Diameter of side column	9.0 m	112.5 mm
Draft	20.0 m	250 mm
Displacement	7.351 ton	14.300 kg
Distante from main to side columns	25.4 m	317.5 mm
KG	14.0 m	175 mm
Gyradius Rxx and Ryy	25.8 m	322 mm
Gyradius Rzz	20.7 m	259 mm

2. METHODOLOGY

This study consisted in 3 parts. The first one was the experimental tests, in which the inline force and displacement results were obtained. The numerical approach started by making a verification of the computational methods and postprocessing procedures through the comparison with the result obtained for a single cylinder in oscillatory motion reported in the literature (Dütsch, Durst, Becker, & Lienhart, 1998). After obtaining satisfying agreement with these, two-dimensional simulations for the platform pillars cross-section were carried out, obtaining also the inline hydrodynamic force and coefficients.

According to Tatsuno & Bearman (1990), oscilating flows can be classified according to 2 parameters, the Stokes, β, and Keulegan Carpenter, KC, numbers.

$$KC = \frac{2\pi A}{D}, \tag{1}$$

$$\beta = \frac{fD^2}{\nu} \tag{2}$$

In these expressions, A is the amplitude of motion, D is the characteristic dimension (cylinder diameter), f is the frequency of oscillation, and ν is the kinematic viscosity. The equivalent Reynolds number can be easily obtained by

$$Re = \beta(KC), \tag{3}$$

For this study, we adopted Morison's equation to describe the inline forces actuating on the body. Morison's equation (Morison, O'Brien, & Schaaf, 1950) is given by,

$$F(t) = -\frac{1}{2}\rho D c_d U|U| - \frac{1}{4}\pi\rho D^2 c_i \dot{U}, \tag{4}$$

with,

$$U(t) = -A\omega\cos(\omega t), \ \omega = 2\pi f \tag{5), (6}$$

The term proportional to the velocity is related to the viscous drag and the term proportional to the acceleration is related to the inertial forces. The respective c_d and c_i are the drag and added mass or inertia coefficients.

To obtain the values of the force coefficients, we employed the procedure presented by Keulegan & Carpenter (1958). Since the viscous and inertial terms have different phases, it is possible to obtain the drag and added mass force components through a Fourier analysis. We can represent the total force by

$$F_{total}(t) = A_0 + \sum_1^\infty [A_n \cos(n\omega t) + B_n \sin(n\omega t)], \tag{7}$$

$$A = \frac{1}{T}\int_0^T F(t)\,dt\,, \tag{8}$$

$$A_n = \frac{2}{T}\int_0^T F(t)\cos(n\omega t)\,dt\,, \tag{9}$$

$$B_n = \frac{2}{T}\int_0^T F(t)\sin(n\omega t)dt\,. \tag{10}$$

Since we are assuming that the signal follows the behavior of Morrison's equation, we know that $A_0 = 0$. Furthermore, the acceleration proportional component is a simple sine function and therefore can be easily represented by a single term

$$F_{inertia}(t) = -\frac{1}{4}\pi\rho D^2 c_i \dot{U} = b_1 \sin(\omega t), \tag{11}$$

$$b_1 = \frac{2}{T}\int_0^T F(t)\sin(\omega t)dt\,, \tag{12}$$

On the other hand, the viscous force has the form $|\cos(wt)|\cos(wt)$ which cannot be simply represented with a Fourier series as its inertial counterpart. However, it can be written as

$$|\cos(wt)|\cos(\mathrm{wt}) = a_0 + a_1\cos(wt) + a_2\cos(2wt) + a_3\cos(3wt) + \cdots, \tag{13}$$

for which we find that the even terms are all zero and the odd terms can be written as

$$a_n = \frac{(-1)^{\frac{n+1}{2}}8}{n(n^2-4)\pi}\,. \tag{14}$$

To linearize the problem, aiming simplification, we neglect the higher terms and only the first one is used,

$$a_1 = \frac{8}{3\pi}, \tag{15}$$

so that,

$$|\cos(wt)|\cos(\mathrm{wt}) \sim a_1\cos(wt). \tag{16}$$

Therefore, we can rewrite the total inline force as

$$F(t) = A_1'\cos(\mathrm{wt})\,|\cos(\mathrm{wt})\,| + b_1\sin(\omega t), \tag{17}$$

with,

$$A_1' = \frac{A_1}{a_1}. \tag{18}$$

The force coefficients can then be obtained comparing equations (4) and (17). (Sarpkaya, 1986) also defined the coefficient c_f as a parameter to compare the total inline force, as

$$c_f = \left(\frac{3}{8}c_d^2 + \frac{\pi^4 c_i}{2(KC)^2}\right)^{\frac{1}{2}}. \tag{19}$$

2.1 Experimental setup

The tests were conducted at the wave basin of the Numerical Offshore Tank of the University of São Paulo (TPN-USP), shown in Figure 2. It is a squared 14 m x 14 m x 4 m (length, width, depth) tank equipped with 152 active-absorption flap-type wave generators that can generate incident waves and absorb the ones produced by the model (Mello, et al., 2013). The hull model was built in a 1:80 scale considering Froude scaling, and its main properties are given in Table 1.

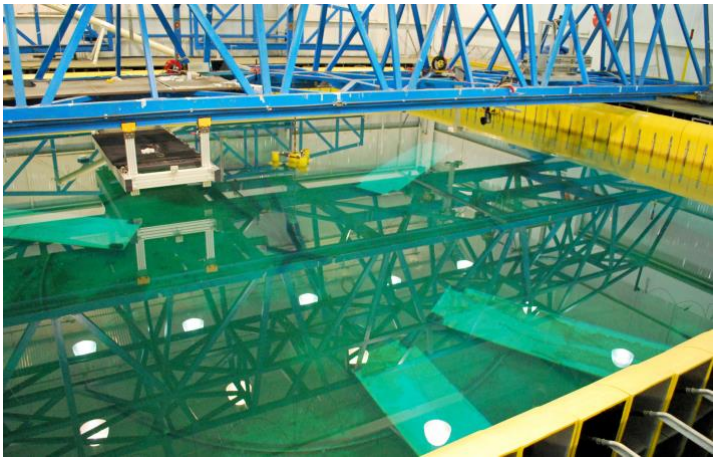

Figure 2. Wave basin of the Numerical Offshore Tank of the University of São Paulo (TPN-USP).

For the experiments discussed in this text, a linear actuator was assembled at the center of the tank, as illustrated in Figure 3. The model was attached to the actuator and forced to move horizontally following a prescribed sinusoidal motion with the amplitudes and period listed in Table 2 and Table 3. The period of 12 s was chosen to represent the typical period of ocean waves, while 84.4 s is the natural period of surge motion of the floater. The additional value of 60 s was included to assess the forces for an intermediate period that is within the range of possible surge resonance periods of floating wind turbines. The amplitudes of motion were established based on estimations of surge motion amplitudes that could be expected in real seas, which were later confirmed with experiments considering the floater under the action of waves (Carmo, et al., 2020), (Amaral, et al., 2021). The time series of the force exerted by the actuator was measured using a set of four load cells with a capacity of 100N assembled between two parallel plates, with a sampling rate of 100 Hz.

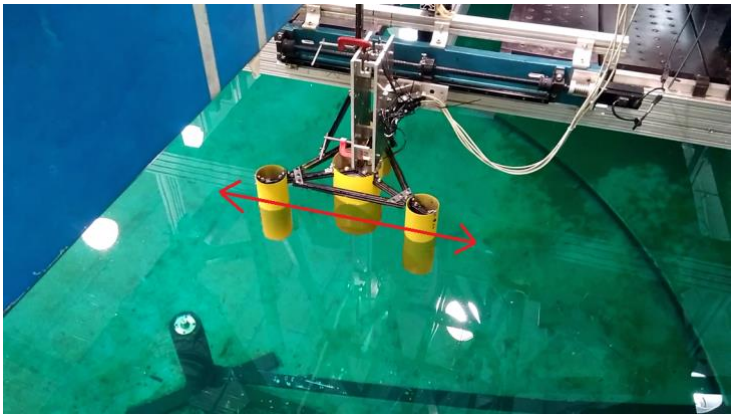

Figure 3. Setup of the forced oscillation tests. Direction of movement as indicated by the red arrow.

Table 2. Motion amplitudes of the forced oscillations and corresponding KC values.

Amplitude (m)		**KC**
Real scale	Model scale	
0.800	0.010	0.48
1.600	0.020	0.96
2.400	0.030	1.44
3.200	0.040	1.91
4.000	0.050	2.39
4.800	0.060	2.87

Table 3. Motion periods considered in the forced oscillations and the corresponding β values.

Period (s)		**β**
Real scale	Model scale	
12.0	1.34	12740.97
60.0	6.71	2544.40
84.4	9.43	1810.49

2.2 Numerical simulations

The Computational Fluid Dynamics (CFD) simulations were performed in 2 dimensions using the open-source software OpenFOAM, which employs the finite volume method to compute the flow (Weller, Tabor, Jasak, & Fureby, 1998). The velocity-pressure coupling was made using the PIMPLE method, which is a combination of the well-established PISO and SIMPLE algorithm (Robertson, Choudhury, & S. Bhushan, 2015). No turbulence model was employed. To simulate the oscillating flow, we chose to work with the inertial reference frame, which is the same used in the experiments, and therefore a movable mesh had to be utilized. Even being computationally more expensive, this method was more direct to apply, and, on a two-dimensional domain, it did not become a problem. For the velocity and pressure fields, we considered a zero gradient boundary condition for the left and right boundaries and a symmetry condition for the top and bottom ones. The mesh was generated using the software Ansys (ANSYS, 2020) and then converted to the OpenFOAM mesh format. A mesh convergence test was performed to ensure grid independence.

2.2.1 Single cylinder simulations

The simulations of the flow around a single oscillating cylinder were performed to validate the method. The computational domain had the length of 30 diameters in the direction of the oscillation and of 20 diameters in the orthogonal direction and the final mesh had 12172 elements, as shown in figure 4. Three cases were considered to verify the flow patterns, as presented in Table 4, and 9 cases to verify the force coefficients agreement, as shown in Table 5.

Table 4. Flow pattern comparison cases.

β	**KC**
20	5 10
35	6

Table 5. Force coefficients comparison cases.

β	KC
35	0.5 1 1.5 2 3 4 5 6 7

2.3 Plataform cross section simulations

For the calculation of the force coefficients, we considered the weighted average diameter, $D_m = 132.25$ mm. The considered simulation domain had a length of 30 D_m and a width of 20 D_m, and a mesh with 10307 elements was utilized, as shown in Figure 5. The simulations employed the same β and KC parameters range as the experimental tests.

The experimental force signals were preprocessed to remove the noise. To do so, we applied the Fast Fourier Transform (FFT) algorithm on the signal to obtain the frequency components, removed those that were not of interest and then applied the inverse FFT (iFFT) to get the signal back to the time domain.

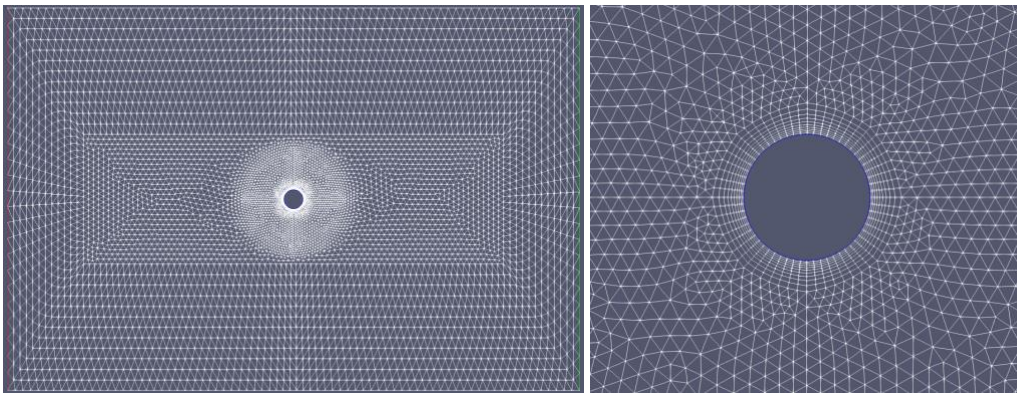

Figure 4. Single cylinder mesh.

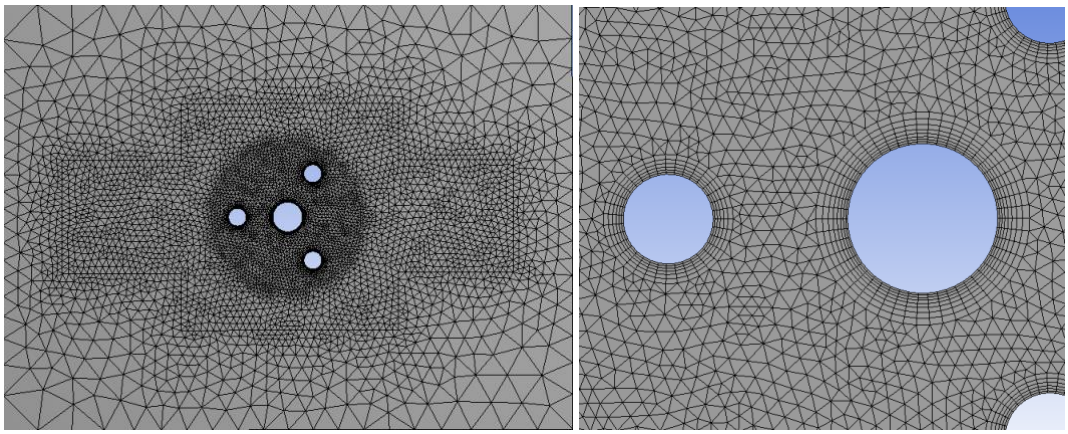

Figure 5. Platform cross-section mesh.

3. VERIFICATION AND VALIDATION

To verify if the methodology applied in the simulations and the post-processing techniques were valid, we utilized the results presented by Dütsch, Durst, Becker, & Lienhart (1998) as a reference for the comparison of the flow field and force coefficients. The pressure and vorticity fields are compared for three different cases and are shown in Figure 6. We can see that there is a good agreement between the reference and new numerical simulations.

For the comparison of the forces and force coefficients, we generated a reference force signal using the force coefficients presented by Dütsch, Durst, Becker, & Lienhart (1998) applied to Morison's equation (4). The decomposition and rebuilt methods were verified by computing the mean squared error between the original numerical signal and the reconstructed signal using the Keulegan & Carpenter (1958) method, it can be verified in Figure 7(b). We

can see that there is a good agreement between the numerical input and the rebuilt signals, except for the KC = 7 case. That happened because the obtained numerical force input was quite irregular, but when we applied the decomposition techniques, the resultant force coefficients were in good agreement with the reference values. Overall, the drag coefficients were usually smaller for the new numerical simulations, while the added mass coefficients were larger, which resulted in a slightly higher total force for the new numerical simulations.

Figure 8 shows the results for the force coefficients. As we can see, they are in good agreement with the reference values.

3.1 Validation

When analyzing the platform results, we note the same behavior presented in the single cylinder simulations. The drag forces captured on the numerical simulation are significantly lower than the ones found experimentally, but, on the other hand, the added mass forces are higher, as we can see from the force coefficients in Figure 9.

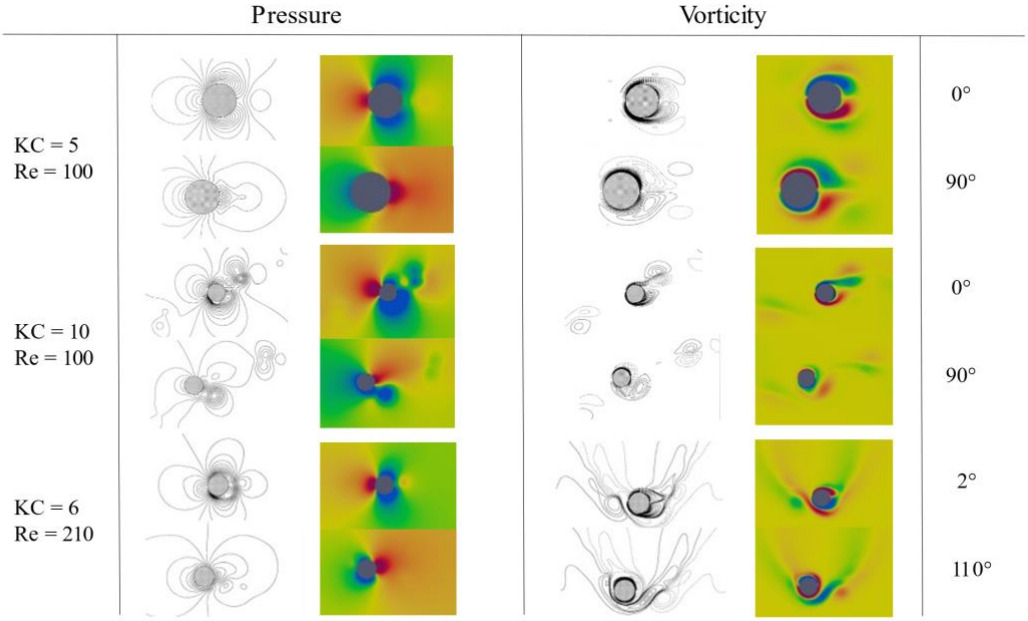

Figure 6. Pressure and velocity field. Reference (Dütsch, Durst, Becker, & Lienhart, 1998) (left) and new simulations (right).

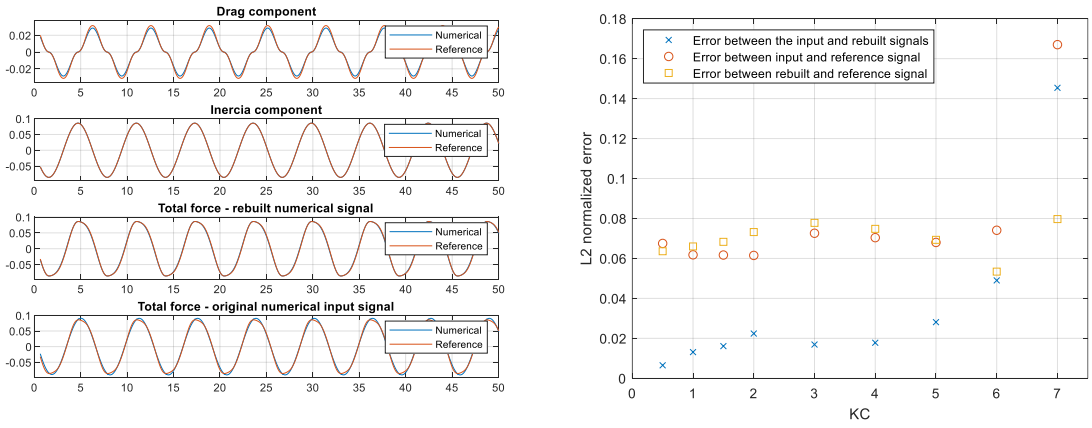

(a) (b)

Figure 7. (a) Illustration of the force decomposition (KC = 0.5; β = 35); (b) L2 normalized error.

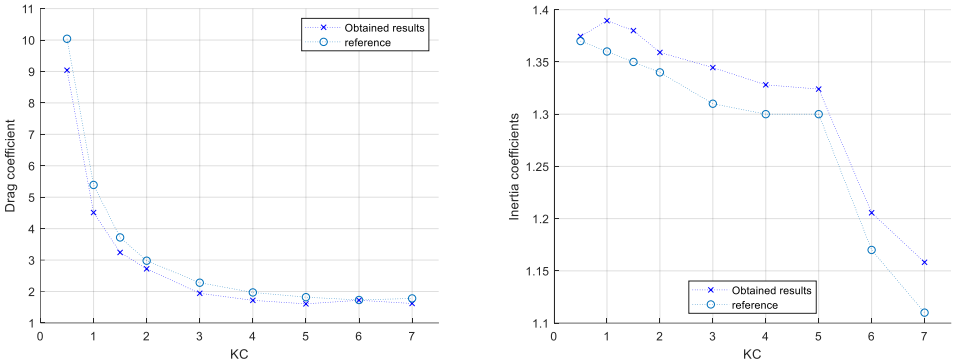

(a) (b)

Figure 8. New numerical results and reference values for the c_d(a) and c_i (b).

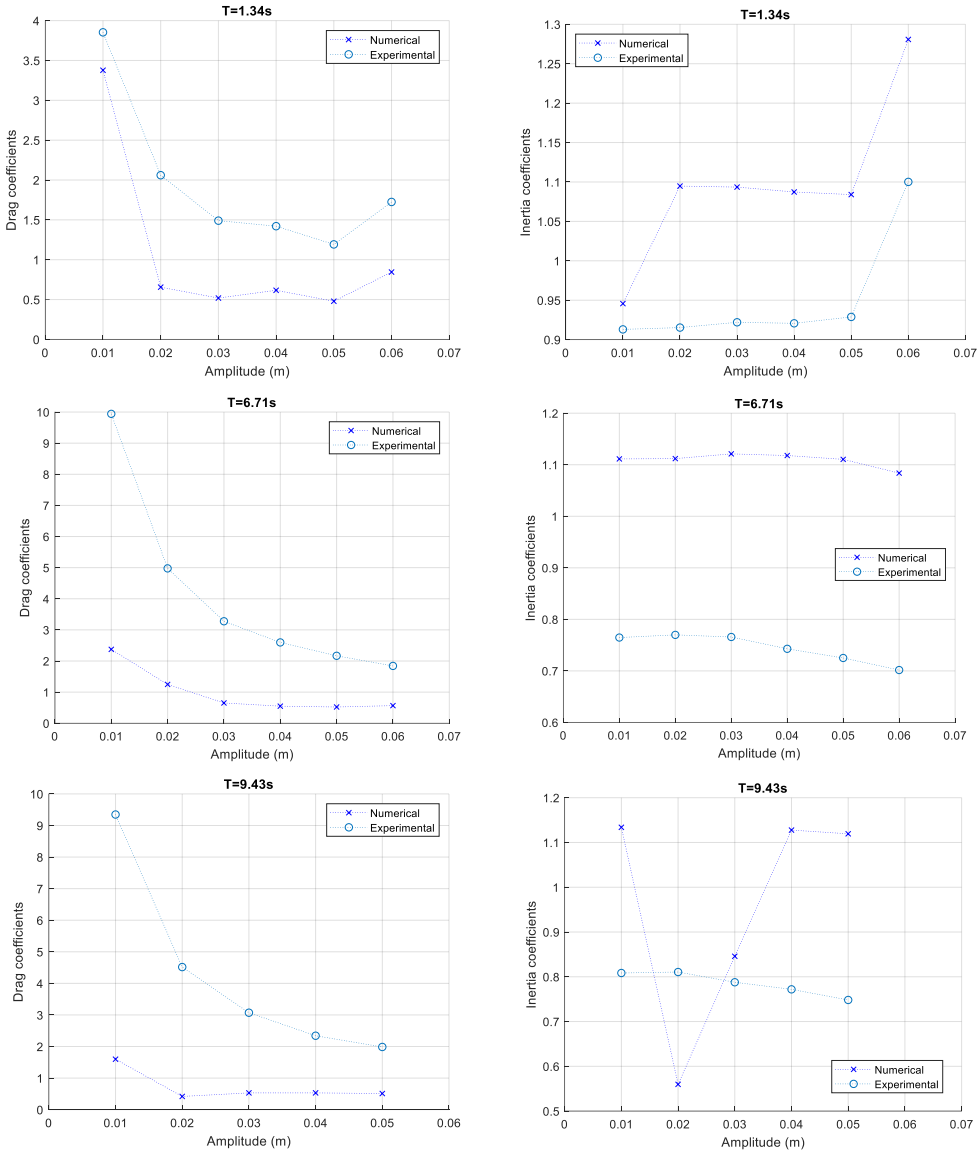

Figure 9. Force coefficient values computed from the numerical and experimental data.

On the other hand, we can see in Figure 10 that there is a good agreement between the experimental and numerical c_f values, showing that the total inline force obtained by the numerical method is coherent. We can also analyze the difference between the maximum amplitude of the numerical and experimental results. From that, it is possible to see a

significant difference between the rebuilt and original experimental signal, which is not observed in the numerical data. That can be explained by the presence of noise in the experimental data which have frequencies that are not accounted by the decomposition technique. Therefore, the unprocessed data (with the filter applied) shows a better agreement than the decomposed and rebuilt data, which is maybe a sign that the decomposition might not be good in these cases. The results were better for the smaller periods and were particularly good for the case T = 1.34 s and A=0.01 m.

The c_f pattern follows the tendency presented by Sarpkaya (1986), who showed that the c_f values are proportional to the inverse of the KC number. This is evident in the graphs shown in Figure 11.

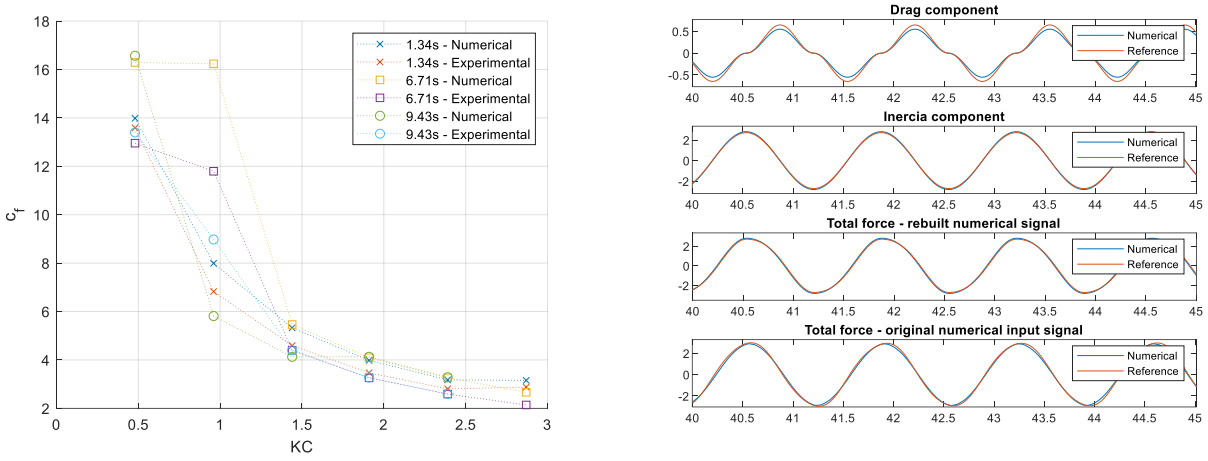

(a) (b)

Figure 10. (a) c_f *values* related to KC; (b) best case decomposition visualization.

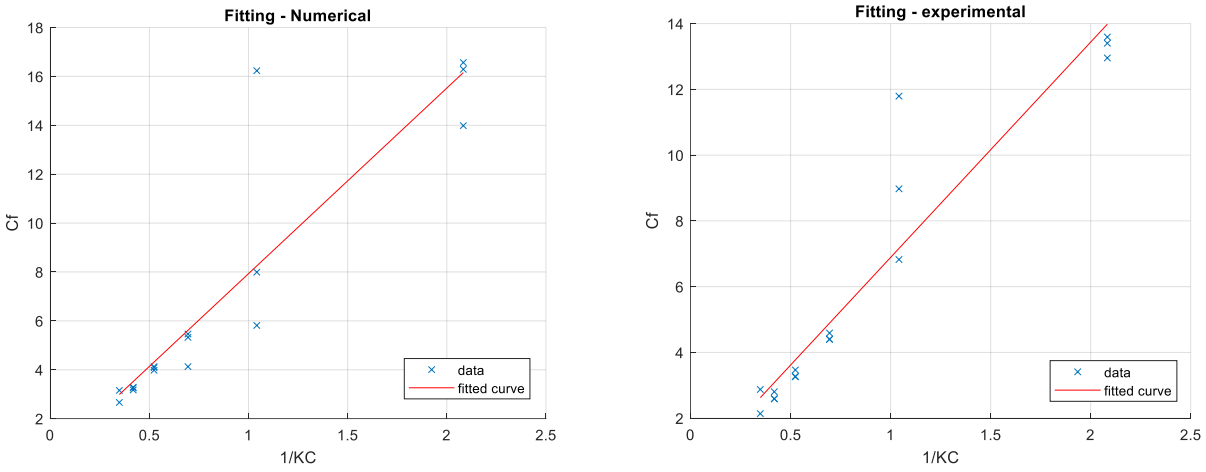

Figure 11. Data fitting of the c_f coefficient plotted against the inverse of the Keulegan-Carpenter number (KC).

4. CONCLUSIONS

The results obtained for the single cylinder cases were quite satisfactory and corroborates with the statement of Dütsch, Durst, Becker, & Lienhart (1958) that it is possible to represent the flow characteristics of a low KC and low β with two-dimensional simulations.

The comparison with the experimental results related to the Jappaku platform, in one way, did not have as quite as satisfying results, as the inertia and drag coefficients obtained were quite different, especially for the higher periods. On the other hand, the total inline force showed an exceptionally good agreement. This is a very interesting result as we noted that this discrepancy between drag and inertia coefficients were also observed in the single cylinder cases but were amplified on the platform cases. As a result, we can suppose that the two-dimensional simulation yielded good results, but the decomposition methods were not adequate for the higher stokes number cases. As a next step, it would be interesting to perform three-dimensional simulations to evaluate this statement.

5. ACKNOWLEDGEMENTS

This work was developed as part of the R&D project conducted by Petrobras and the University of São Paulo entitled "Research and Development on Deep Water Floating Offshore Wind Turbines" (agreement Petrobras #5900.0112605.19.9). Authors wish to thank Petrobras for the funding of this project and the Brazilian National Petroleum Agency (Agência Nacional do Petróleo, ANP) for providing the regulatory framework under which this funding takes place. The FOWT concept adopted in this work was developed in the context of the Brazil-Japan collaborative research project titled "Development of a new solution for floating offshore wind turbines - Jappaku FOWT", financed by the Brazilian Coordination for the Improvement of Higher Education Personnel (CAPES) and the Japan Society for Promotion of Science (JSPS). B. S. Carmo acknowledges financial support from the Brazilian National Council for Scientific and Technological Development (CNPq) in the form of productivity grant (grant number 312951/2018-3).

6. REFERENCES

Amaral, G. A., Mello, P. C., Carmo, L. H., Alberto, I. F., Malta, E. B., Simos, A. N., . . . Gonçalves, R. T. (2021). Seakeeping Tests of a FOWT in Wind and Waves: An Analysis of Dynamic Coupling Effects and Their Impact on the Predictions of Pitch Motion Response. *Journal of Marine Science and Engineering, 9*(2), 179.

ANSYS, I. (2020). ANSYS Meshing User's Guide.

Bilgili, M., Yasar, A., & Simsek, E. (2011). Offshore wind power development in Europe and its comparison with onshore counterpart. *Renewable and Sustainable Energy Reviews, 15*(2), 905 - 915.

Carmo, L. H., Mello, P. C., Malta, E. B., Franzini, G. R., Simos, A. N., Gonc¸alves, R. T., & Suzuki, H. (2020). Analysis of a FOWT model in bichrimatic waes: an investigation on the effect of combined wave frequency and slow motions on the calibration of drag and inertial force coefficients. *Proceedings of the ASME 2020 39th International Conference on Ocean, Offshore and Arctic Engineering.* Fort Lauderdale, Florida, USA: OMAE2020.

Dütsch, H., Durst, F., Becker, S., & Lienhart, H. (1998). Low-Reynolds-number flow around an oscillating circular cylinder at low Keulegan-Carpenter numbers. *Journal of Fluid Mechanics, 360*, 249-271.

Keulegan, G. H., & Carpenter, L. H. (1958). Forces on Cylinders and Plates in an Oscillating Fluid. *Journal of Research of the National Bureau of Standards, 60*(5), 423 - 440.

Lee, J., Zhao, F., Dutton, A., Backwell, B., Fiestas, R., Qiao, L., . . . Younger, D. R. (2021). *GLOBAL WIND REPORT 2021.* Brussels, Belgium: Global Wind Energy Council.

Mello, P. C., Carneiro, M. L., Tannuri, E. A., Kassab Jr., F., Marques, R. P., Adamowski, J. C., & Nishimoto, K. (2013). A control and automation system for wave basins. *Mechatronics, 23*(1), 94-107.

Robertson, E., Choudhury, V., & S. Bhushan, D. W. (2015). Validation of OpenFOAM numerical methods and turbulence models for incompressible bluff body flows. *Computers and Fluids, 123*, 122-145.

Sarpkaya, T. (1986). Force on a circular cylinder in viscous oscillatory flow at low Keulagen-Carpenter Numbers. *Journal of Fluid Mechanics, 165*, 61-71.

Sun, X., Huang, D., & Wu, G. (2012). The current state of offshore wind energy technology development. *Energy, 41*(1), 298 - 312.

Tatsuno, M., & Bearman, P. W. (1990). A visual study of the flow around an oscillating circular cylinder at low Keulegan-Carpenter numbers and low Stokes numbers. *Journal of Fluid Mechanics, 211*, 157 - 182.

Weller, H. G., Tabor, G., Jasak, H., & Fureby, C. (1998). A tensorial approach to computational continuum mechanics using object-oriented techniques. *Computers in Physics, 12*, 620 - 631.

7. RESPONSIBILITY NOTICE

The authors are the only responsible for the printed material included in this paper.